Analytical Hybrid Quasi-3D Transformer Leakage Inductance Model

Analytical Hybrid Quasi-3D Transformer Leakage Inductance Model

Richard Schlesinger, *Student Member, IEEE*, Thomas Ewald, *Student Member, IEEE*, and Jürgen Biela, *Senior Member, IEEE*

***Abstract*—Fast and accurate models of the transformer leakage inductance are crucial for optimisation-based design of isolated converters. This paper proposes an analytical Hybrid Quasi-3D (HQ3D) model for E/U/ER/UR-core type transformers that combines the best-suited submodels for each winding section of the transformer. A submodel is developed that directly calculates the leakage inductance contribution of curved winding sections based on the integration of the radially weighted magnetic energy density. The HQ3D model can describe arbitrary winding positions and its fully analytical nature guarantees optimal geometrical scalability. The only restriction is that the windings need to be parallel to the core edges. The HQ3D model is in the accuracy range of 3D FEM and verified with measurements on nine transformer prototypes with significantly different geometry ranges. The HQ3D model is rapidly executable and therefore well-suited for optimisations of galvanically isolated converters.**

***Index Terms*—Analytical transformer leakage inductance model, Hybrid models, Quasi-3D, Double-2D, Optimisation, Isolated converters**

I. Introduction

LEAKAGE INDUCTANCE is an important property of transformers in isolated power electronic converters. Isolated converters are key elements in several applications that enable more sustainable energy systems such as photovoltaic inverters [1] and electric traction systems [2]. These converters are usually designed with an optimisation that iterates the converter's properties such as losses, efficiency, and the transformer leakage inductance using appropriate models of these properties [1]–[3]. Such optimisations can take up to several thousands of recalculations [3]. Hence, the employed models do not only have to be accurate, they also have to be computationally efficient to deliver results within a reasonable amount of time.

Analytical models fulfil the trade-off between accuracy and computational efficiency well and are therefore a favourable choice for optimisations [4]. Formulating a general analytical 3D leakage inductance model directly is barely possible since E-core and U-core transformer geometries feature rather complex geometries and materials with different permeability need to be modelled. Hence, analytical leakage inductance models are typically based on splitting the geometry into one or multiple basic cross sections as shown in Figs. 1a–c. The most common way to calculate the leakage inductance from the cross sections is to calculate leakage inductances per unit length of each 2D cross section, multiply them by their particular partial length, and sum up the products [4], [5].

1D-models are only based on the inside-window cross section shown in Fig. 1b [6]–[12] and assume that the magnetic field only has an axial component that is solely dependent on the radial coordinate (axial: y-coordinate, radial: x-coordinate in Fig. 1b). This assumption leads to substantial errors when the winding heights are not in the same range as the core window height [4]. Furthermore, they are not directly applicable to windings with different heights as the magnetic field strength can only depend on one height in the 1D assumption. Recent leakage inductance models [4], [13]–[17] pursue a Double-2D concept, i.e. the calculation is based on the inside-window (IW) and the outside-window (OW) cross section as depicted in Figs. 1b&c. In [13], 2D FEM is used for calculating the inductances per unit length, which is accurate but computationally expensive, making it suboptimal for optimisations. In [15], the winding conductors are modelled individually, which also leads to high accuracy but rather high computational effort. Many models [13]–[16] use geometrical mean lengths (mean length of turns, average winding length) to scale the inductances per unit length. However, as inductance is proportional to magnetic energy, geometrically averaged lengths lead to errors for curved winding sections [5] (winding sections with diagonally hatched background in Fig. 2). In contrary to straight winding sections (winding sections showcased with rectangular pattern in Fig. 2), a radially energy weighted mean length has to be used for curved winding sections due to the curvature of the magnetic field [5]. In [17], an energy-weighted

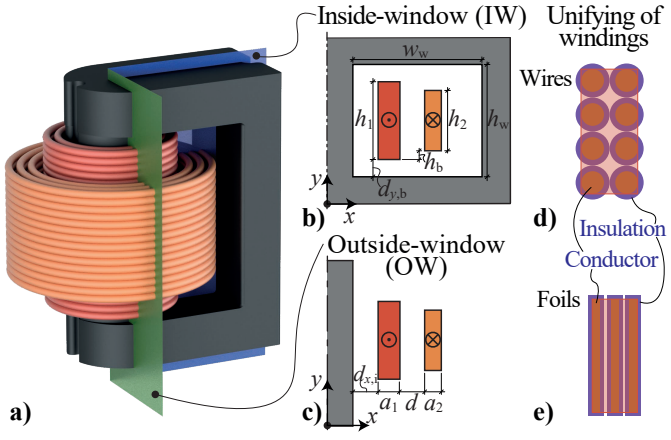

Fig. 1: **a)** Exemplary transformer geometry. **b)** Inside-window (IW) cross section. **c)** Outside-window (OW) cross section. **d)&e)** Unifying of wire and foil windings to conductor blocks.

Richard Schlesinger (schlesinger@hpe.ee.ethz.ch), Thomas Ewald (ewald@hpe.ee.ethz.ch) and Jürgen Biela (jbiela@ethz.ch) are with the Laboratory for High Power Electronic Systems, ETH Zurich.

mean length is proposed but the assumed geometry features winding corners bent at right angles instead of continuously curved winding corner sections. This assumed geometry leads to an erroneous amount of stored magnetic energy as it neglects the winding curvature. Furthermore, it is restricted to cores with rectangular center leg. Some models use cylindrical coordinates to implicitly take into account the curvature of the field in curved winding sections [18], [19]. But these solutions are complex to derive and involve computationally effortful evaluations of Bessel integrals. Furthermore, these models are not applicable to straight winding sections and hence, not applicable to cores with rectangular center legs. In [20], an accurate Triple-2D model for transformers with circular center legs is proposed comprising a third cross section – the transition region (TR) between IW and OW plane. Taking the TR plane into account leads to slightly lower errors by the prize of having to model three instead of two cross sections. Furthermore, the magnetic energy integrals in model [20] need to be numerically evaluated leading to high computational costs. Ultimately, many useful models exist but all of them lack either physical accuracy, geometrical versatility, or computational efficiency making them suboptimal for optimisations.

Therefore, this paper proposes an accurate and rapidly executable Hybrid Quasi-3D (HQ3D) model that is designed to fill this void. The HQ3D model is defined by two characteristics: First, the HQ3D model follows a quasi-3D concept, i.e. the leakage inductance contribution of the curved winding sections is directly calculated from the leakage inductance per unit angle scaled by the corresponding section angle. Here, the leakage inductance per unit angle is derived by integrating the radially weighted magnetic energy density. Thus, the radial energy weighting required in curved winding sections is implicitly taken into account, which is an advantage of the Quasi-3D concept in comparison to the Double-2D concept. The second characteristic of the HQ3D model is that for each winding section, the best suited models are used, hence the term ”hybrid”. In particular, the HQ3D model uses an analytical solution of the leakage inductance per unit angle proposed in this paper for curved winding sections. The proposed expression is derived from Roth’s field expression [21] and implemented in a computationally efficient way using array operations in Matlab. For straight winding sections, the most accurate & computationally efficient models are selected based on a previously performed comparison [4]. In particular, Roth’s model [21] is used for the IW cross section and the model of Margueron et al. [22] is used for the OW cross section. The resulting HQ3D model stands out by offering fully analytical solutions to calculate the leakage inductance of transformers with curved as well as straight winding sections such as E/U/ER/UR-core transformers and many more. The position of the windings is completely arbitrary and the analytical solutions guarantee full geometrical scalability. The HQ3D model is verified with 3D-FEM simulations and measurements on nine transformer prototypes.

This paper is structured as follows: First, the Quasi-3D and Double-2D modelling concepts are presented, and their differences are highlighted in section II. Section III derives expressions of magnetic energy from the magnetic vector potential

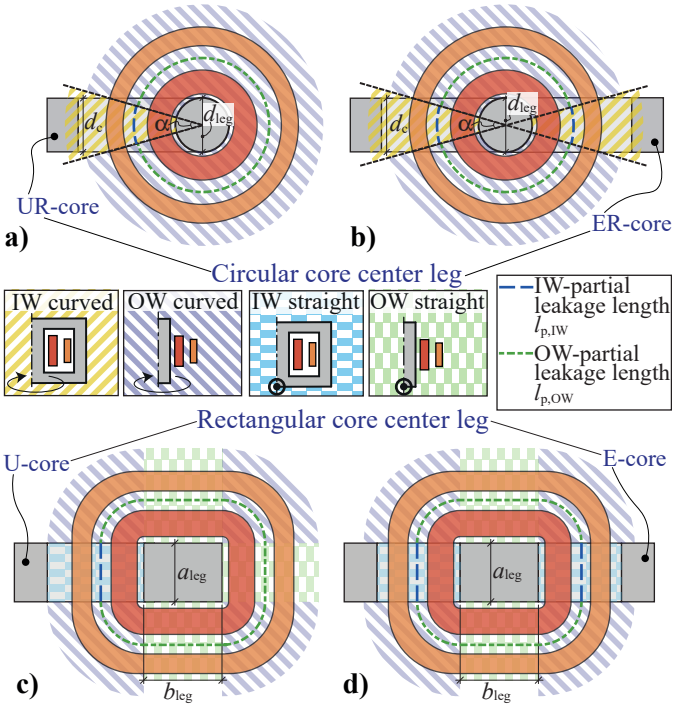

Fig. 2: Elementary winding sections of considered transformer types. Curved winding sections are emphasised with a diagonally hatched background whereas straight winding sections are highlighted with a rectangular pattern. The blue dashed line and the green dot-dashed line represent the partial leakage lengths required in the Double-2D modelling concept. **a)** UR-core, **b)** ER-core, **c)** U-core, **d)** E-core.

that are required for leakage inductance calculation. Section IV presents the proposed HQ3D leakage inductance model. The HQ3D model is verified with measurements and 3D FEM in section V. Section VI shows that frequency effects play an insignificant role for leakage inductance when carefully designing technical transformers. The Appendix presents the newly derived leakage inductance per unit angle from Roth’s potential expression and an alternative Hybrid Double-2D (HD2D) model.

II. Analytical Leakage Inductance Modelling Concepts

This section summarises the Double-2D and Quasi-3D modelling concept and elaborates necessary fundamental considerations. Both concepts are based on the two basic transformer cross sections: inside-window (IW) and outside-window (OW) shown in Figs. 1b&c. The transformer is modelled by calculating leakage inductance contributions from IW and OW winding sections, both of which can be either curved or straight as shown in Fig. 2. The composition of winding sections depends on the core type used in the transformer. In Fig. 2, curved winding sections are diagonally hatched whereas straight winding sections are emphasised with a rectangular pattern. The two presented concepts differ in the way how the contribution of curved winding sections is taken into account as elaborated below.

A. Double-2D Modelling Concept

The Double-2D leakage inductance modelling concept is performed in the steps below:

1) IW and OW leakage inductances per unit length $L'_{\sigma,\mathrm{IW}}$ and $L'_{\sigma,\mathrm{OW}}$ are calculated from the IW and OW cross sections shown in Figs. 1b&c.
2) Scaling lengths are calculated for IW and OW cross section. These scaling lengths are referred to as IW and OW partial leakage lengths $l_{\mathrm{p,IW}}$ and $l_{\mathrm{p,OW}}$. The partial leakage lengths depend on the transformer type as each transformer type consists of different elementary winding sections (cf. Figs. 2 and 3). Note that the partial leakage lengths can comprise both straight and curved winding sections as indicated with the dashed and dash-dotted lines in Fig. 2.
3) The total leakage inductance is obtained according to (1).

$$\underbrace{L_{\sigma,\text{Double-2D}}}_{\text{3D}} = \underbrace{L'_{\sigma,\mathrm{IW}}}_{\text{2D}}\,\underbrace{l_{\mathrm{p,IW}}}_{\text{1D}} + \underbrace{L'_{\sigma,\mathrm{OW}}}_{\text{2D}}\,\underbrace{l_{\mathrm{p,OW}}}_{\text{1D}} \tag{1}$$

The leakage inductances per unit length L'_σ from step 1) are calculated via the surface integral of the magnetic energy density according to (2).

$$L'_\sigma = \frac{2}{I_{\mathrm{ref}}^2} W'_{\mathrm{mag}} = \frac{2}{I_{\mathrm{ref}}^2} \iint_{\mathcal{A}} w_{\mathrm{mag}}\,\mathrm{d}A \tag{2}$$

Where W'_{mag} is the magnetic energy per unit length, I_{ref} is the current through the excited winding, and w_{mag} is the magnetic energy density. In the Double-2D concept, curved winding sections (diagonally hatched winding sections in Fig. 2) are treated the same way as straight sections, hence the curvature of the magnetic field is neglected in the first step. The field curvature is only taken into account in the next step by using the radially energy weighted mean length (leakage length l_σ referring to the 360° rotation of the respective cross section [5]. The leakage length is calculated according to (3).

$$l_\sigma = \frac{W_{\mathrm{mag,rotated}}}{W'_{\mathrm{mag}}} = \frac{2\pi \iint_{\mathcal{A}} x\, w_{\mathrm{mag}}(x,y)\,\mathrm{d}A}{\iint_{\mathcal{A}} w_{\mathrm{mag}}(x,y)\,\mathrm{d}A} \tag{3}$$

As curved winding sections are typically smaller than 360° (cf. Fig. 2), appropriate fractions of the leakage length are used to take into account the contribution of the particular curved winding section. Note when calculating the leakage inductance contribution of a (360°-portion of a) curved winding section, one receives

$$L_{\sigma,\mathrm{curved}} = L'_\sigma\, l_\sigma = \frac{2}{I_{\mathrm{ref}}^2} 2\pi \iint_{\mathcal{A}} x\, w_{\mathrm{mag}}(x,y)\,\mathrm{d}A,$$

which contains the radially-weighted energy integral $\iint_{\mathcal{A}} x\, w_{\mathrm{mag}}(x,y)\,\mathrm{d}A$. This integral describes the per-unit-angle contribution of a curved winding section and is significantly harder to compute analytically than the per-unit-length integral $\iint_{\mathcal{A}} w_{\mathrm{mag}}(x,y)\,\mathrm{d}A$ without the radial (x) weighting in the integrand. Therefore, typically approximative models are used to calculate the leakage length (3). These are usually subject to strong simplifications, which makes them simple but also imposed by geometrical restrictions (e.g. two concentric windings, only valid within certain geometric aspect ratios) [5]. The more difficult but cleaner approach of solving the radially energy-weighted integral $\iint_{\mathcal{A}} x\, w_{\mathrm{mag}}(x,y)\,\mathrm{d}A$ directly is the fundamental property of the Quasi-3D concept introduced in the following section.

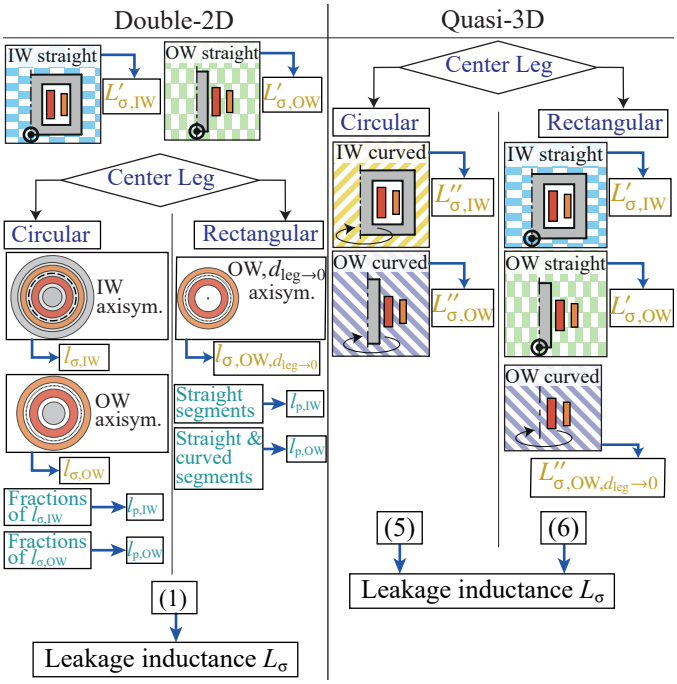

Fig. 3: Double-2D & Quasi-3D modelling concepts. Elementary quantities that require a submodel to compute are shown in gold.

B. Quasi-3D Modelling Concept

The Quasi-3D modelling concept introduced in this paper is distinguished by directly calculating the leakage inductance contribution of curved winding sections without taking the detour via the energy weighted mean length as in the Double-2D concept. In particular, the leakage inductances per unit angle L''_σ of the curved winding sections are calculated and scaled by the corresponding section angle. L''_σ is obtained by integrating the radial coordinate multiplied by the magnetic energy density according to (4) and therefore implicitly takes the field curvature in curved winding sections.

$$L''_\sigma = \frac{2}{I_{\mathrm{ref}}^2} W''_{\mathrm{mag}} = \frac{2}{I_{\mathrm{ref}}^2} \iint_{\mathcal{A}} x\, w_{\mathrm{mag}}\,\mathrm{d}A \tag{4}$$

Where W''_{mag} is the magnetic energy per unit angle and x is the radial coordinate (x-coordinate in Figs. 1b&c).
As mentioned before, the transformer consists of different elementary winding sections (i.e. curved or straight sections – cf. Fig. 2) depending on the core type. Hence, the Quasi-3D concept distinguishes between cores with rectangular and circular center leg as shown in Fig. 3.

1) Quasi-3D for circular center legs: In transformers with a circular core center leg, the leakage inductance according to the Quasi-3D concept is calculated with (5)

$$L_{\sigma,\text{Quasi-3D}} = L''_{\sigma,\mathrm{IW}}\, s_{\mathrm{core}}\, \alpha + L''_{\sigma,\mathrm{OW}}\,(2\pi - s_{\mathrm{core}}\,\alpha). \tag{5}$$

Where $\alpha = 2 \arcsin\left({}^{d_\mathrm{c}}/_{(d_\mathrm{leg}+2d_{x,\mathrm{i}}+2a_1+2d+2a_2)}\right)$ [5] is the IW section angle in radians shown in Figs. 2a&b, in which also the core depth d_c and the center leg diameter d_leg are defined. $d_{x,\mathrm{i}}$ is the distance between inner winding and center leg, a_1 and a_2 are the primary and secondary winding width, respectively, and d is the distance between the windings as shown in Fig. 1c. s_core denotes the number of windows of the core.

$$s_\mathrm{core} = 1 \text{ (UR- and U-core)} \qquad s_\mathrm{core} = 2 \text{ (ER- and E-core)}$$

2) Quasi-3D for rectangular center legs: In transformers with a rectangular core center leg, the leakage inductance according to the Quasi-3D concept is calculated with (6).

$$\begin{aligned} L_{\sigma,\text{Quasi-3D}} = {} & L'_{\sigma,\text{IW}}\, s_\mathrm{core}\, a_\mathrm{leg} + L'_{\sigma,\text{OW}}(2b_\mathrm{leg} + (2 - s_\mathrm{core})a_\mathrm{leg}) \\ & + L''_{\sigma,\text{OW},d_\mathrm{leg}\to 0}\, 2\pi \end{aligned} \tag{6}$$

Where a_leg and b_leg are the center core leg depth and width, respectively as shown in Figs. 2c&d. The leakage inductance contribution of straight winding sections is calculated by multiplying L'_σ by the length of the straight winding section – same as in the Double-2D concept. Note also that with rectangular center legs, the windings are only curved around the center leg's corners as shown in Figs. 2c&d. For each corner section, the center of rotation is located directly at the corner of the center leg, hence $d_\mathrm{leg} \to 0$ in the calculation of the OW-leakage inductance per unit angle $L''_{\sigma,\text{OW},d_\mathrm{leg}\to 0}$ for rectangular center legs.

C. General Assumptions of Leakage Inductance Models

1) Balanced magnetomotive forces: To obtain the magnetic leakage field, the magnetomotive forces of the windings are assumed to be equal in magnitude but opposite in direction.

2) Unifying of conductors to blocks: Unifying the conductors of each winding to rectangular blocks drastically reduces the geometric complexity of the magnetic field calculation while maintaining high accuracy [20]. In particular, the windings are unified such that the winding block's boundaries coincide with the outermost dimensions of the conductors as shown in Figs. 1d&e. Also, rectangular winding blocks are required to apply the models of Roth [21] and Margueron et al. [22] which are both used in this paper.

3) Homogeneous current distribution: All analytical models used in this paper assume homogeneous current distribution in the windings. This is a reasonable assumption as leakage inductance is directly proportional to magnetic energy – a macroscopic quantity. As macroscopic quantity, the local redistributions due to skin- and proximity effect can be neglected for a soundly designed technical transformer. Further details on this can be found in section VI.

III. Expressions of Magnetic Energy

This section derives expressions of the magnetic energy per unit length (p.u.l.) and magnetic energy per unit angle (p.u.a.) required for computing the leakage inductance p.u.l. L'_σ (2) and leakage inductance p.u.a. L''_σ (4). This is done by replacing the magnetic flux density $\vec{B}$ and magnetic field strength $\vec{H}$ with the magnetic vector potential $\vec{A}$ and current density $\vec{J}$. Since the basic cross sections – IW and OW, cf. Figs. 1b&c – only comprise through-plane current densities in z-direction, the vector potential and current density only have a z-component $\vec{A}(x,y) = A_z(x,y)\vec{e}_z$. The magnetic flux density can be derived from the magnetic potential with $\vec{B} = \vec{\nabla} \times \vec{A}$. The calculation via the magnetic potential is favourable as the problem is reduced from a vector problem ($\vec{B}$, $\vec{H}$-field) to a scalar problem ($A_z(x,y), J_z(x,y)$).

A. Leakage Inductance Per Unit Length (p.u.l.)

The leakage inductance p.u.l. of a given cross section can be calculated with the magnetic energy p.u.l. as given in (2). To facilitate some simplifications, we reformulate the magnetic energy density introducing the magnetic vector potential and using vector identity 7 in [23, ch. 11.2] resulting in (7).

$$w_\mathrm{mag} = \frac{1}{2}\vec{B}\cdot\vec{H} = \frac{1}{2}\left[\vec{\nabla}\cdot(\vec{A}\times\vec{H}) + \vec{A}\cdot\vec{J}\right] \tag{7}$$

where $\vec{H}$ is the magnetic field strength and $\vec{J}$ is the current density. The magnetic energy p.u.l. can be calculated with the surface integral of the magnetic energy density using Gauss's law, which yields (8).

$$W'_\mathrm{mag} = \iint_{\mathcal{A}} w_\mathrm{mag}\,\mathrm{d}A = \frac{1}{2}\left[\oint_{\partial\mathcal{A}} \vec{n}\cdot(\vec{A}\times\vec{H})\,\mathrm{d}s + \iint_{\mathcal{A}} \vec{A}\cdot\vec{J}\,\mathrm{d}A\right] \tag{8}$$

The contribution of the boundary integral in (8) is determined by the imposed boundary conditions that depend on the considered cross section, i.e. IW or OW. For both cross sections, the integrand of the boundary integral becomes zero $\vec{n}\cdot(\vec{A}\times\vec{H}) = 0$ as explained below.

In the IW-cross section (cf. Fig. 1b), the conductors are enclosed by a high permeability material, hence $\mu_r \to \infty$ is a good assumption and the field lines of $\vec{H}$ are orthogonal to the boundary (mirroring boundary condition – Neumann BC). The vector potential $\vec{A}$ is through-plane only. Hence, the cross product $\vec{A}\times\vec{H}$ can only have tangential components at the boundary and therefore, the projection on the normal vector is zero over the total boundary $\vec{n}\cdot(\vec{A}\times\vec{H}) = 0$.

In the OW cross section (cf. Fig. 1c), the inner boundary represents a mirroring boundary condition and the other boundary conditions represent a magnetic insulation boundary condition (Dirichlet BC) of boundaries that are infinitely far away. The two windings with balanced magnetomotive forces have dipole character for distances sufficiently far away from the windings. In dipoles, the magnetic field $\vec{H}$ decreases with ${}^1/_{r^3}$ and the potential $\vec{A}$ decreases with ${}^1/_{r^2}$ with r being the distance to the dipole [24]. Hence, the product $\vec{A}\times\vec{H}$ decreases with ${}^1/_{r^5}$, whereas the integration sector (perimeter) only scales with r. Hence, the integral $\oint_{\partial\mathcal{A}} \vec{n}\cdot(\vec{A}\times\vec{H})\,\mathrm{d}s$ vanishes at the infinite boundary at $r \to \infty$.

Consequently, the magnetic energy per unit length for IW and OW cross section can be calculated with (9).

$$W'_\mathrm{mag} = \frac{1}{2}\iint_{\mathcal{A}} \vec{A}\cdot\vec{J}\,\mathrm{d}A \tag{9}$$

The above equation (9) is a very common approach used in numerous leakage inductance models [21], [22], [25], [26] and the leakage inductance per unit length can be derived from it using (2).

B. Leakage Inductance Per Unit Angle (p.u.a.)

The leakage inductance p.u.a. of the IW and OW cross section can also be derived using the magnetic potential, which is shown in the following. The magnetic energy p.u.a. is derived via the integral of the radial coordinate multiplied by the magnetic energy density from (7) according to (10).

$$\begin{aligned} W''_{\text{mag}} &= \iint_{\mathcal{A}} x \; w_{\text{mag}} \, \mathrm{d}A \\ &= \frac{1}{2} \left[\underbrace{\iint_{\mathcal{A}} x \left(\vec{\nabla} \cdot (\vec{A} \times \vec{H}) \right) \, \mathrm{d}A}_{\text{Int}_1} + \iint_{\mathcal{A}} x (\vec{A} \cdot \vec{J}) \, \mathrm{d}A \right] \end{aligned} \tag{10}$$

The first integral Int_1 in (10) can be reformulated using vector identity 6 of [23, ch. 11.2] and Gauss's law as follows

$$\begin{aligned} \text{Int}_1 &= \iint_{\mathcal{A}} \vec{\nabla} \cdot \left(x \; (\vec{A} \times \vec{H}) \right) - \left(\vec{A} \times \vec{H} \right) \cdot \vec{\nabla} x \, \mathrm{d}A \\ &= \oint_{\partial \mathcal{A}} \vec{n} \cdot (x (\vec{A} \times \vec{H})) \, \mathrm{d}s + \iint_{\mathcal{A}} H_y A_z \, \mathrm{d}A \end{aligned}$$

The integral $\oint_{\partial \mathcal{A}} \vec{n} \cdot (x(\vec{A} \times \vec{H})) \, \mathrm{d}s$ again only depends on the boundary conditions. As the scalar field x does not change the direction of the vector field $(\vec{A} \times \vec{H})$, its normal projection on the boundary still vanishes at boundaries with mirroring boundary condition ($\mu_\text{r} \to \infty$). For Dirichlet-boundaries in infinity, the product $x(\vec{A} \times \vec{H})$ decreases with $1/r^5$ in axial direction (y) and with $1/r^4$ in radial direction (x) due to the dipole character of the field. Hence, the integral $\oint_{\partial \mathcal{A}} \vec{n} \cdot (x(\vec{A} \times \vec{H})) \, \mathrm{d}s$ again vanishes at the infinite boundary considering that the integrand decays with at least $1/r^4$ whereas the integration sector only increases with r (see also section III-A).
Hence, the magnetic energy per unit angle in IW and OW cross section can be calculated with (11)

$$\begin{aligned} W''_{\text{mag}} &= \frac{1}{2} \left[\iint_{\mathcal{A}} x (\vec{A} \cdot \vec{J}) \, \mathrm{d}A + \iint_{\mathcal{A}} H_y A_z \, \mathrm{d}A \right] \\ &= \frac{1}{2} \left[\iint_{\mathcal{A}} x (\vec{A} \cdot \vec{J}) \, \mathrm{d}A - \frac{1}{2\mu} \iint_{\mathcal{A}} \frac{\partial}{\partial x} (A_z^2) \, \mathrm{d}A \right] \end{aligned} \tag{11}$$

The leakage inductance p.u.a. can then be derived from the magnetic energy p.u.a. in (11) with (4). This paper proposes an analytical derivation of the magnetic energy per unit angle W''_{mag} given in Appendix A-D using the magnetic potential expression of Roth [21]. This analytical solution of W''_{mag} is the key element in the Hybrid Quasi-3D model which is proposed in the following section IV.

IV. Hybrid Quasi-3D Leakage Inductance Model

This chapter presents the proposed Hybrid Quasi-3D (HQ3D) leakage inductance model. The HQ3D model is based on the Quasi-3D modelling concept presented in section II-B and uses the specific set of submodels given in Tab. I for the magnetic energy expressions derived in section III. In particular, the HQ3D model combines different best suited submodels for the elementary quantities depicted in Fig. 3, hence the term "hybrid". All submodels used in the HQ3D model are analytical, which leads to the big advantage that they can be applied to any winding geometry with windings parallel to the core edges as the analytical solutions guarantee scalability to arbitrary geometric aspect ratios.

Table I: Submodels of the proposed Hybrid Quasi-3D (HQ3D) model.

Quantity	Chosen submodel	Reference
$L''_{\sigma,\text{IW}}$	Proposed expression (12)	Appendix A-D
$L''_{\sigma,\text{OW}}$	Proposed expression (12)	Appendix A-D
$L''_{\sigma,\text{OW},d_\text{leg}\to 0}$	Proposed expression (12)	Appendix A-D
$L'_{\sigma,\text{IW}}$	Roth (13)	[21]
$L'_{\sigma,\text{OW}}$	Margueron et al. 2010	[22]

As discussed in section II-B, the Quasi-3D concept is distinguished by implicitly taking into account the curvature of the magnetic field of curved winding sections by using the leakage inductance per unit angle L''_σ of the particular cross section. In The HQ3D model, L''_σ is calculated according to (12),

$$\begin{aligned} L''_\sigma &= \frac{h_\text{w} w_\text{w}^2}{4 \, I_\text{ref}^2} \\ &\left[\sum_{m=1}^{M} A_{m0} \tilde{J}_{m0} + \sum_{n=1}^{N} A_{0n} \tilde{J}_{0n} + \frac{1}{2} \sum_{m=1}^{M} \sum_{n=1}^{N} A_{mn} \tilde{J}_{mn} \right] \end{aligned} \tag{12}$$

where h_w and w_w are window height and window width, respectively, I_ref is the current through the excited winding, and A_{mn} is given in Appendix A-A. The expression (12) is derived in Appendix A-D which also contains the coefficients $\tilde{J}_{mn}$.
For straight winding sections, existing analytical models are selected based on their excellent trade-off between accuracy and computational effort [4]. In particular, the IW leakage inductance per unit length is calculated with Roth's per unit length model [21] according to (13).

$$\begin{aligned} L'_{\sigma,\text{IW}} &= \frac{h_\text{w} w_\text{w}}{2 \, I_\text{ref}^2} \\ &\left[\sum_{m=1}^{M} A_{m0} J_{m0} + \sum_{n=1}^{N} A_{0n} J_{0n} + \frac{1}{2} \sum_{m=1}^{M} \sum_{n=1}^{N} A_{mn} J_{mn} \right] \end{aligned} \tag{13}$$

The derivation of this equation and the coefficients A_{mn} and J_{mn} are given in Appendix A-A. The originally infinite series are approximated with M and N spatial harmonics in (12) and (13), respectively, which is valid as the summands of the series converge very rapidly with $1/m^4$. The number of spatial harmonics required for satisfactory accuracy is elaborated in the following subsections.
The OW leakage inductance per unit length $L'_{\sigma,\text{OW}}$ is calculated with the model of Margueron et al. [22]. This model is based on a Green's function as analytical solution of the Poisson equation and uses discrete mirror images to take into account the impact of the core on the magnetic field. Since there is only one mirror image in the OW cross section [4], the model is compact and rapidly computable. The equations of the model of Margueron et al. can be found in the original publication [22] and in the supplementary document of [4].

A. Convergence of Roth's Series

This section introduces necessary considerations to evaluate how many spatial harmonics M and N are required for

satisfactory convergence of (12) and (13). Please note that details are omitted here to get an overview of the mathematical problem. Instead, some forward-references are made to round up the picture.

First, it needs to be examined which factors define the convergence of the series in these equations. Here, it is important to remind that the first step in Roth's derivation [21] is to express the current density $J_{z,\mathrm{k}}$ of each winding k and its mirror images as a double spatial Fourier series as shown in (17) in Appendix A. As the current density in the windings is assumed to be homogeneous, this essentially equals approximating a rectangular periodic signal by a double Fourier series in space (see also Fig.9 in the supplementary document of [4]). Just like when approximating a rectangular periodic signal in time domain, the convergence is optimal for a duty cycle of $\delta = 0.5$, representing the ratio of the time when the signal is non-zero to the total period. Convergence becomes worse when the duty cycle approaches 0. In the considered application of double Fourier series, two spatial duty cycles $\delta_{x,\mathrm{k}}$ and $\delta_{y,\mathrm{k}}$ can be defined for each winding k according to (14).

$$\delta_{x,\mathrm{k}} = a_k / w_\mathrm{w} \qquad \delta_{y,\mathrm{k}} = h_k / h_\mathrm{w} \tag{14}$$

Where a_k and h_k are width and height of winding k, respectively, and w_w and h_w are width and height of the transformer window, respectively. Hence, the current density tends to converge best when the winding covers half of the window width and height. The same is also true for the magnetic potential $A_{z,\mathrm{k}}$ that is derived from the current density via Poisson's equation according to (20).

After reformulations given in Appendix A, the leakage inductance per unit angle L''_σ and leakage inductance per unit length L'_σ are obtained as triple sum and as double sums, respectively as shown in (12) and (13). These multidimensional sums are only dependent on the spatial Fourier coefficients of current density $J_{k,mn}$ and magnetic potential $A_{k,mn}$.

All of these sums have the prefactor $1/m^4$ and $1/n^4$ in common, hence convergence is guaranteed. Predictions on convergence however, are hindered by the following two obstacles.

1) The overall Fourier coefficients are determined via superposition of the Fourier coefficients of all windings according to (21). Hence, the convergence of the sums always depends on multiple windings and the interaction (constructive or destructive interference) of their spatial Fourier coefficients.
2) The summands of the multidimensional series contain products of terms that depend on the individual summation indexes. Therefore, there is an interaction of the sums representing the different space-coordinates. This interaction can increase or decrease overall convergence.

All in all, a generalised prediction of convergence is therefore not possible. However, two important conclusions can be drawn from this section:

- Spatial duty cycles (14) close to 0 tend to decrease convergence.
- Due to the factor $1/m^4$, the series always converge. Hence, the sums can be approximated with a finite number of spatial harmonics.

Based on these general considerations, the number of spatial harmonics M and N used in the present implementation for IW and OW cross section are deduced in section IV-C. Before that however, it is necessary to present some model adaptions required for the OW cross section.

B. Adapting Roth's Model to the OW Cross Section

Roth's magnetic potential and current density expressions are tailored to the IW cross section shown in Fig. 1b as they implicitly satisfy the imposed mirroring boundary conditions at all surrounding window edges. To use the model for the OW cross section in which the boundary conditions are different, a simple trick is applied: the windings are placed in an equivalent window whose width and height are significantly larger than the original window with the intention of representing an infinitely large window as also done in [19]. It is important to note that the windings are kept at center height. Also, the distance of the inner winding to the center leg $d_{x,\mathrm{i}}$ is kept constant as this distance is the same in IW and OW cross section as shown in Figs. 1b&c. As a consequence, the winding-yoke distances $d_{y,\mathrm{b}}$ and $d_{y,\mathrm{t}}$ and the outer winding-leg distance $d_{x,\mathrm{o}}$ (cf. Fig. 9c) are modelled as infinitely large such that they do not affect the magnetic field anymore.

An equivalent window that is bigger than the original window leads to smaller spatial duty cycles $\delta_{x,\mathrm{k}}$ and $\delta_{y,\mathrm{k}}$. As elaborated in section IV-A, spatial duty cycles close to 0 tend to decrease the convergence of (12) and (13). Hence, the equivalent window should be small enough to keep convergence at reasonable levels. At the same time, the equivalent window has to be as big as necessary to eliminate the influence of the core yokes and outer leg on the magnetic field. Specifically, the equivalent window's width and window height are increased linearly by a factor c until a certain maximum spatial duty cycle of the windings according to (15) is reached.

$$\delta_\mathrm{max} = \max_k \left\{ {}^{a_k}\!/_{(c\,w_\mathrm{w})}, {}^{h_k}\!/_{(c\,h_\mathrm{w})} \right\} \tag{15}$$

The maximum duty cycle present in the transformer is taken in this regard as this corresponds to minimum winding-yoke distances that could still affect the magnetic field. To evaluate the limit for δ_max, the leakage inductance per unit length L'_σ and leakage inductance per unit angle L''_σ in dependence of δ_max are shown in Fig. 4 for nine exemplary transformer prototypes. The prototypes cover a wide range of winding/core geometries as shown in section V and Tab. VI and therefore cover a wide range of convergence behaviours. Fig. 4 reveals that L'_σ and L''_σ stay constant if δ_max falls below 0.2 for any of the tested transformer prototypes. The figure has been created by gradually increasing width and height of the equivalent window, i.e. by gradually increasing factor c in (15). Based on this, $\delta_\mathrm{max} = 0.2$ is set to model the OW cross section in the HQ3D model. Note that based on this finding, scaling window width and window height by a factor of $c = 2$ as done in [19] might not be sufficiently large to eliminate the influence of the core on the magnetic field to a satisfactory degree.

C. Number of Spatial Harmonics in Roth's Model

This section analyses how many spatial harmonics M and N are required in the series of (12) and (13). Generally, the

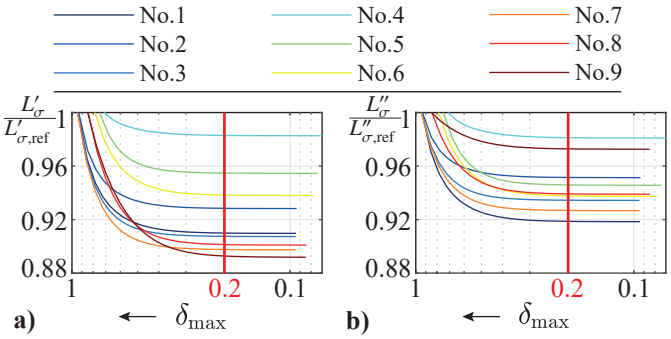

Fig. 4: Relative decrease of leakage inductance for decreasing maximum spatial duty cycles (15) of the transformer prototypes listed in Tab. VI. The IW leakage inductance calculated with 2D FEM is chosen as the reference leakage inductance. If $\delta_{\max}$ falls below 0.2, the results stay constant because here the core is too far away from the windings to significantly affect the magnetic field. **a)** Leakage inductance per unit length. **b)** Leakage inductance per unit angle.

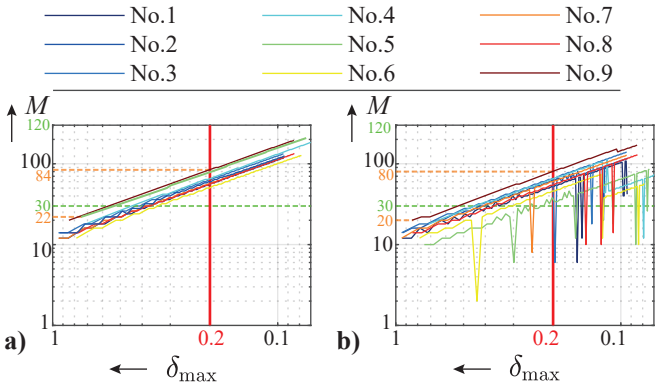

Fig. 5: Required number of spatial harmonics to obtain a maximum tolerance of $\epsilon = 1\text{e}{-3}$. **a)** Leakage inductance per unit length L'_σ. **b)** Leakage inductance per unit angle L''_σ.

number of harmonics should be as low as possible for quick computation, and at the same time as high as necessary to ensure satisfactory accuracy. First, $M = N$ is assumed to simplify the analysis. Satisfactory accuracy shall be reached as soon as enough harmonics are summed up that the result lies within a maximum error tolerance of $\epsilon = 10^{-3} = 0.1\,\%$ in comparison to the reference value acquired with 2D FEM according to (16).

$$\left\{\left|{}^{L_\sigma(M)'}/_{L'_{\sigma,\text{2DFEM}}}-1\right|,\ \left|{}^{L_\sigma(M)''}/_{L''_{\sigma,\text{2DFEM}}}-1\right|\right\} \leq \epsilon,\ \ \epsilon = 10^{-3} \tag{16}$$

Figs. 5a&b show the number of spatial harmonics required to land within the defined error tolerance for L'_σ and L''_σ, respectively for all 9 transformer prototypes. The initial maximum duty cycle $\delta_{\max}$ at the leftmost end of each curve in Fig. 5 corresponds to the IW cross section. Here, an error below $0.1\,\%$ is achieved with 12 to 22 harmonics for L'_σ and with 10 to 20 harmonics for L''_σ. To include a safety margin, $M_{\text{IW}} = 30$ spatial harmonics are chosen in the calculation routine of the IW cross section.

Starting from the initial $\delta_{\max}$, the equivalent window's width

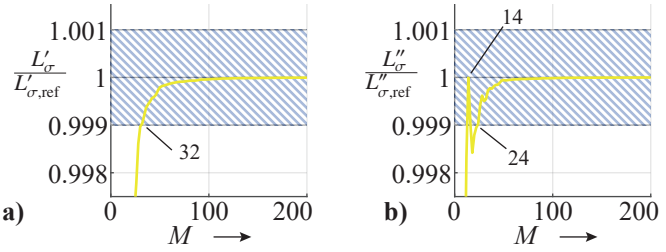

Fig. 6: Exemplary worst-case convergence of leakage inductance of transformer prototype No.6 in an equivalent window whose width and height are 5 times bigger than the original window (corresponding to $\delta_{\max} = 0.19$). The blue surface depicts the convergence tolerance $(1-\epsilon) \leq {}^{L_\sigma}/_{L_{\sigma,\text{ref}}} \leq (1+\epsilon)$. **a)** Leakage inductance per unit length (13). **b)** Leakage inductance per unit angle (12).

and height are gradually increased and the corresponding maximum spatial duty cycle $\delta_{\max}$ is plotted on the abscissa. The previous subsection showed that $\delta_{\max} < 0.2$ corresponds to constellations representing the OW cross section. At $\delta_{\max} = 0.2$, between 50 and 84 harmonics are required to achieve errors below $0.1\,\%$ for L'_σ. For L''_σ, 36 to 80 harmonics are required to get smaller errors than $0.1\,\%$. To also add a safety margin here, $M_{\text{OW}} = 120$ spatial harmonics are chosen in the OW cross section calculation routine. Apart from the chosen number of spatial harmonics, two things are also to conclude from Fig. 5.

First, the figure shows that duty cycles approaching 0 demand a higher number of spatial harmonics to achieve satisfactory accuracy. This confirms that the convergence of both, (12) and (13) gets worse for duty cycles approaching 0, which was already stated in section IV-A. Hence, applications with particularly low spatial duty cycles such as individual lanes in PCB transformers might require some more spatial harmonics to achieve satisfactory accuracy. In such cases, Fig. 5 can be used as reference to see how many harmonics are required for a transformer with a certain $\delta_{\max}$.

Second, it is also noteworthy that the spatial duty cycle has a different influence on the required spatial harmonics when comparing L'_σ to L''_σ. Looking at the leakage inductance per unit length L'_σ in Fig. 5a, the number of required spatial harmonics increases quite continuously with decreasing maximum spatial duty cycle. This is because the series (13) contains the Fourier coefficients (18) that can be positive or negative only in squared form. Hence, the individual sum terms can only be positive leading to a monotonous convergence to the final value as shown in Fig. 6a. In the series yielding the leakage inductance per unit angle (12), the Fourier coefficients (18) do not appear in a squared form. Therefore, the individual sum terms can be negative as well as positive. As a consequence, the series might not converge monotonically but can also oscillate before the final value is reached as shown in an exemplary worst-case scenario in Fig. 6b. This is also the cause of the fluctuations in the number of required spatial harmonics over the changing spatial duty cycle for L''_σ shown in Fig. 5b. Unfortunately, the oscillating behaviour of the series

Table II: Chosen parameters in the proposed leakage inductance per unit angle expression (12) and Roth's leakage inductance per unit length expression (13) deduced from considerations of sections IV-B and IV-C.

	IW	OW
$M = N$ in (12) and (13)	30	120
$\delta_{\max}$ (15)	given by geometry	0.2

Table III: Relative error of proposed analytical leakage inductance per unit angle L''_σ expression (12) using the parameters in Tab. II in relation to 2D FEM.

	No.1	No.2	No.3	No.4	No.5	No.6	No.7	No.8	No.9
IW	-0.009%	-0.009%	-0.008%	-0.022%	-0.016%	-0.008%	-0.093%	-0.008%	-0.024%
OW	0.016%	0.003%	0.001%	0.004%	0.008%	0.029%	-0.073%	0.029%	0.043%

convergence cannot be predicted in a reasonably simple and general way due to the interaction of Fourier coefficients of different windings and space directions mentioned in section IV-A. Nevertheless, convergence is guaranteed in both cases due to the factor of $1/m^4$ in both series (12) and (13). Tab. II summarises the essential model parameterisations required for Roth's model that were deduced in the two previous sections.

V. Model Verification

This section verifies both, the proposed leakage inductance per unit angle expression (12) and the proposed HQ3D model presented in section IV. Nine transformer prototypes given in Tab. VI provide reference geometries for the verification. The transformers cover a variety of cores and aspect ratios to maximise the significance of the presented results.

A. Verification of Leakage Inductance Per Unit Angle Expression

First, the proposed leakage inductance per unit angle L''_σ expression (12) derived in Appendix A-D is verified by comparing the results of (12) with the results of 2D FEM simulations of all nine transformer prototypes in Tab. III. The table shows that the error of the proposed L''_σ-expression (12) is close to zero in all geometries in both IW and OW cross section. This proves that the analytical derivation of the equation executed in Appendix A-D is correct and that the number of chosen spatial harmonics in Tab. II is sufficient. Furthermore, the maximum spatial duty cycle of $\delta_{\max}$ in the OW cross section was chosen small enough.

Fig. 7 shows convergence and calculation time data of transformer No.8 and further underlines the accuracy of the presented model. The proposed L''_σ calculation (12) in Fig. 7b converges very well to the reference value calculated with 2D FEM. Unsurprisingly, the IW calculation converges faster than the OW calculation due to the smaller spatial duty cycle of the windings. Note that the L'_σ calculation (13) shown in Fig. 7a converges in a very similar way. Hence, not every geometry leads to convergence oscillations in L''_σ such as the worst-case example in Fig. 6b.

It is noteworthy that the calculation time of L'_σ scales

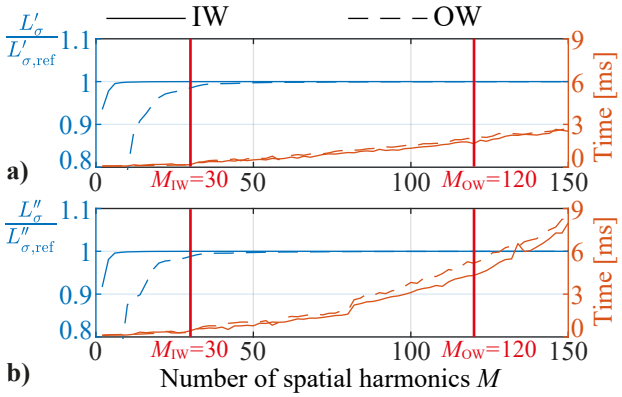

Fig. 7: Left axis: convergence of L'_σ (13) and L''_σ (12) for transformer No.8. The number of chosen harmonics M for IW and OW are marked in red. Right axis: required execution time extracted with the Matlab profiler.

with $\mathcal{O}(M^2)$ as the algorithm consists of summing up 2-dimensional arrays representing the double series in (13). The calculation time of L''_σ, however, increases with $\mathcal{O}(M^3)$ as the algorithm sums up 3-dimensional arrays representing the triple series in (12).

B. Verification of Hybrid Quasi-3D Leakage Inductance Model

The results of the proposed HQ3D leakage inductance model are compared with 3D FEM simulations and measurements of the nine transformer prototypes in Tab. IV. In a first step, the 3D FEM simulations are taken as benchmark for model verification because they feature the exact same geometry that is modelled in the HQ3D model. In particular, the windings are modelled as unified blocks with the geometries listed in Tab. VI to serve as reference for the mathematical reformulations executed throughout the model derivation. Hence, error resulting from geometric tolerances and measurement inaccuracies are not included when comparing with 3D FEM. Tab. IV shows that the average error of the HQ3D model compared with the 3D FEM simulation is below $1\,\%$. Hence, errors in the formulation of the HQ3D model can be excluded as it coincides very well with 3D FEM. The remaining average error of $0.75\,\%$ is primarily caused by the inevitable influence of 3D-transition effects between the considered cross sections. These are neglected a priori when modelling based on multiple 2D cross sections and represent a general limitation in analytical models. The average error of the HQ3D model compared with the measurements is $5.3\,\%$, which is a realistic benchmark on how accurate models can be compared with measurements. This error range of $5\,\%$ to $10\,\%$ is inevitable as measurements are always prone to an error chain resulting from geometric tolerances, measurement inaccuracies, and model simplifications. This statement is supported by the fact that the average error of the 3D-FEM simulations ($4.7\,\%$) in relation to the measurements is in the same range.

Table IV: Leakage inductance results of Hybrid Quasi-3D (HQ3D) and Hybrid Double-2D (HD2D) model compared with 3D FEM and measurement as reference. All leakage inductances are referred to the primary side of the transformers.

	3D FEM			Meas.			
Tr.	L_σ (µH)	**HQ3D**	**HD2D**	L_σ (µH)	**3D FEM**	**HQ3D**	**HD2D**
No.1	27.84	-0.91%	-1.94%	27.00	3.1%	2.2%	1.1%
No.2	10.57	-0.10%	-0.32%	10.70	-1.2%	-1.3%	-1.5%
No.3	13.97	-0.13%	-0.43%	13.40	4.3%	4.1%	3.8%
No.4	9.97	0.06%	0.21%	10.90	-8.5%	-8.4%	-8.3%
No.5	5.59	1.47%	2.28%	5.35	4.5%	6.0%	6.9%
No.6	28.17	0.60%	0.47%	26.60	5.9%	6.5%	6.4%
No.7	14.08	-0.70%	-1.11%	14.30	-1.5%	-2.2%	-2.6%
No.8	50.28	2.11%	1.84%	47.52	5.8%	8.0%	7.8%
No.9	0.317	0.84%	1.22%	0.295	7.5%	8.5%	8.9%
Avg.*	-	0.77%	1.09%	-	4.7%	5.3%	5.3%

*Average $= 1/9 \sum_{n=1}^{9} |L_{\sigma,\mathrm{model},n} - L_{\sigma,\mathrm{ref},n}| / L_{\sigma,\mathrm{ref},n}$

Table V: Comparison of HQ3D and HD2D model

		HQ3D	**HD2D**
Execution time	Circ. center leg	20 ms	34 ms
	Rect. center leg	38 ms	33 ms
Adaptable to arbitrary winding constellations		✓	No*
Applicable to arbitrary geometrical aspect ratios		✓	No**

*Limited to 2 concentric windings
**Limited to geometric aspect ratios listed in Tab. IX

C. Comparison of HQ3D and HD2D Model

The Hybrid Double-2D (HD2D) model presented in Appendix B is slightly less accurate than the HQ3D model when comparing the average error in relation to 3D FEM (1.09 %). This slightly higher error results from using an approximative model to calculate the leakage length, which is typically the case with Double-2D models as metioned in section II-A.

The execution times of the HQ3D model and the HD2D model are both in the range of tens of milliseconds on a standard notebook (Windows 10, Intel i7-8550U processor, 16GB RAM) as shown in Tab. V.[1] Hence, both models are comparable in execution time as well as accuracy.

However, it needs to be pointed out that the fully analytical HQ3D model can describe windings of arbitrary positions as long as the winding edges are parallel to the core edges. The HD2D model on the other hand is restricted to transformers with two concentric windings that are within the geometry range of Tab. IX. The HQ3D model is therefore much more versatile when it comes to geometry.

An interesting aspect to comment is the different performance of HQ3D and HD2D model depending on the shape of the transformer center leg. While the HQ3D might be considered more complex than the HD2D model at first glance, this is not true for transformers with circular center leg. Transformers with circular center leg require only two fundamental quantities in the Quasi-3D modelling concept: $L''_{\sigma,\mathrm{IW}}$ and $L''_{\sigma,\mathrm{OW}}$ (cf. Fig. 3). Both quantities are treated with the same model, hence, the same code is used for both quantities, which is a major advantage. Also, a significant characteristic of the HQ3D model is that the leakage inductance contribution of curved winding sections is directly calculated. In the HD2D model, leakage inductances per unit length L'_σ are calculated as if they were straight winding sections and the radial energy weighting is done in a second step by calculating an energy weighted mean length – the leakage length l_σ. As mentioned, l_σ is usually calculated with approximative models [5]. Hence, the benefits of the HQ3D model over the HD2D model are even more pronounced for transformers with circular center leg.

Transformers with rectangular center leg naturally consist mostly of straight winding sections which are treated the same in the HQ3D and HD2D model. Curved winding sections are only present around the center leg's corners (cf. Figs. 2c&d). Apart from $L'_{\sigma,\mathrm{IW}}$ and $L'_{\sigma,\mathrm{OW}}$, curved winding sections also require $L''_{\sigma,\mathrm{OW},d_{\mathrm{leg}}\to 0}$ in the Quasi-3D concept – which leads to three considerable calculations in the HQ3D model. In contrast, the HD2D model uses a simple energy weighted mean length for the curved winding sections around the center leg's corners and only requires two more extensive calculations for the leakage inductances per unit length. Hence, the complexity regarding implementation of the HQ3D model in case of transformers with rectangular center leg is slightly higher than in the HD2D model. The relative complexity of the models depending on the shape of the transformer center leg is also reflected in the execution times in Tab. V.

VI. Frequency Dependence of Leakage Inductance

Galvanically isolated power converters typically operate in the medium frequency range – usually at a few tens of kHz (e.g. [1], [2]). At these frequencies, skin and proximity effect cause a redistribution of the current density within a conductor. However, in contrary to winding losses, leakage inductance is only affected to a much smaller degree by frequency as it is derived from the stored magnetic energy – a macroscopic quantity that is less affected by local current density variations. The major share of the leakage energy is stored in the air between the windings and is barely affected by current redistributions as the net current through the windings stays constant over frequency. Furthermore, the diameter of the conductors in technical transformers is always designed small enough to limit frequency effects. Typically, the strand diameter should not exceed the skin depth. The assumption of homogeneous current distribution in the analytical models is therefore well justified. Apart from that, analytical models that consider frequency effects are usually based on axial leakage flux assumption [7]–[12]. This leads to considerable error even in the static leakage inductance, especially when the height of the windings is not in the very same range as the core window height [4].

To prove that the impact of frequency on leakage inductance is marginal, three transformers have been designed that have

[1]The time measurement was done with the Matlab profiler to prevent runtime optimisation of Matlab. Note that absolute execution times only give an approximate idea of the computational efficiency of the model. Execution times depend on many additional factors such as the implementation, code overhead, the processor, the programming language, and many more. These factors can change the calculation time even by several orders of magnitude. It is the relative comparison in execution times that brings additional value as the implementation and measurement circumstances were identical here.

Table VI: Data of transformer prototypes. See Figs. 1&2 for geometrical parameter definitions.

	Transformer geometry parameters (mm)													**Further data**					
	a_1	a_2	d	h_1	h_2	h_b	w_w	h_w	$d_{y,\mathrm{b}}$	$d_{x,\mathrm{i}}$	b_leg	a_leg	d_leg	Core	C. leg	N_1	N_2	Wind.1	Wind.2
No.1	4.9	4.9	17.5	90.0	80.0	5.0	34.3	96.0	3.0	0.0	56.0	30.0	-	E	rect.	20	20	Foil	Foil
No.2	4.2	4.6	4.0	52.0	44.0	4.0	20.0	55.8	1.9	0.0	20.2	20.2	-	E	rect.	23	26	Foil	Foil
No.3	3.8	4.5	7.0	48.9	37.9	5.5	23.8	51.9	1.5	0.0	26.0	28.1	-	E	rect.	19	18	Foil	Foil
No.4	4.1	4.3	7.7	72.0	72.0	0.0	31.0	101.0	16.0	3.1	-	-	26.9	UR	circ.	20	1350	Foil	Litz-w.
No.5	2.5	12.0	14.0	72.0	72.0	0.0	47.5	96.4	12.2	3.5	-	-	37.5	UR	circ.	10	952	Foil	Litz-w.
No.6	3.0	6.5	5.0	40.0	37.0	1.5	20.0	51.0	4.5	2.0	-	-	23.4	UR	circ.	32	480	Foil	Litz-w.
No.7	5.2	4.9	6.0	48.9	37.9	5.5	22.9	51.9	1.5	0.0	27.5	27.5	-	E	rect.	19	18	Foil	Foil
No.8	4.0	7.0	3.0	43.0	27.0	8.0	20.0	51.0	4.0	1.5	-	-	23.5	UR	circ.	44	42	Litz-w.	Litz-w.
No.9	1.7	1.8	1.8	38.1	25.4	6.4	11.3	45.0	3.5	1.0	-	-	21.5	ETD	circ.	5	5	Foil	Foil

Table VII: Wire data of transformers No.8a–c.

Tr.	**Number of strands**	**Strand diameter** d_strand (mm)	**Frequency** $\delta_\mathrm{skin} = d_\mathrm{strand}$ (kHz)	**Strands insulated**	**Copper area** (mm^2)
8a	16	0.2	106.3	no	0.50
8b	5	0.355	33.7	✓	0.49
8c	360	0.04	2656.5	✓	0.45

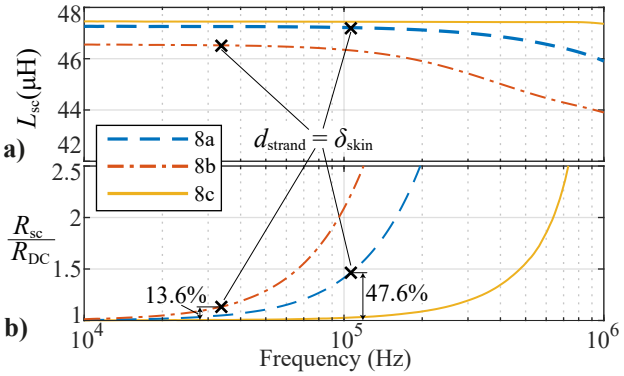

Fig. 8: Short-circuit inductances L_sc and resistances R_sc of transformers No.8a, 8b, and 8c. In the relevant design range (strand diameter d_strand smaller than skin depth δ_skin), the decrease of leakage inductance with frequency is negligible, i.e. below $0.1\,\%$. At the same time, the resistance increase due to frequency is already significant in the tens-of-percent range and therefore two orders of magnitude higher than the drop in leakage inductance. Therefore, technical transformers are usually designed for operating points below that frequency in a regime where leakage inductance is barely affected by frequency effects, which justifies the use of frequency-independent models in the leakage inductance design process. The first resonant capacitance has been compensated as elaborated in Appendix C.

identical cores and identical macroscopic winding dimensions (cf. Tab. VI, transformer No.8). The only difference between the prototypes are their wires. The wires have been selected so that all of them have similar copper cross sections of approx. $0.5\,\mathrm{mm}^2$ and hence similar DC-resistances. The parameters of the three different wires are listed in Tab. VII. Fig. 8 shows the measured short-circuit inductances and winding resistance over frequency of the transformers No.8a–c. The relevant design range is illustrated by marking the corresponding frequencies where the strand diameter equals the skin depth for each transformer with an "x". Technical transformers typically would not be operated at frequencies above that mark as the winding losses would already be significant at this frequency. The figure shows that the measured drop in leakage inductance is below $0.1\,\%$ at the frequency where $d_\mathrm{strand} = \delta_\mathrm{skin}$ whereas the increase in resistance is already in the tens-of-percent range, corresponding to a difference of two orders of magnitude. Hence, in a reasonably designed technical transformer that is operated below that particular frequency, frequency does not significantly affect leakage inductance. This justifies the use of frequency-independent leakage inductance models in the design process.

VII. Conclusion

This paper proposes an accurate & fast Hybrid Quasi-3D transformer leakage inductance model that is verified with measurements and 3D FEM. The Hybrid Quasi-3D (HQ3D) model is fully analytical, and its accuracy is in the range of 3D FEM. In particular, the average error compared with 3D FEM is below $1\,\%$ for the investigated nine transformer prototypes. The average error in comparison with measurements is around $5\,\%$, underlining the accuracy of the HQ3D model. The HQ3D model can describe windings that are arbitrarily placed in the core window, the only restriction is that they need to be parallel to the core edges. The HQ3D uses a newly derived expression of the magnetic energy in curved winding sections to take the curvature of the magnetic field in curved winding sections into account.

Furthermore, a Hybrid Double-2D (HD2D) model is also proposed. The HD2D model is in a similar range regarding accuracy and execution time as the HQ3D model and slightly simpler in some aspects. However, the HD2D model is restricted to two concentric windings within given geometrical bounds. Since the HQ3D model does not have this restriction, the authors recommend to use the HQ3D model.

The paper demonstrates that combining several carefully selected submodels in a hybrid overall-model is a proper approach to obtain an accurate and computationally efficient transformer leakage inductance model. The resulting HQ3D model is also rapidly computable, making it well-suited for optimisation-based design of galvanically isolated converters.

APPENDIX A
DERIVATION OF LEAKAGE INDUCTANCE FROM ROTH'S MAGNETIC POTENTIAL EXPRESSION

This section presents the derivation of leakage inductance per unit angle from the vector potential expression of Edouard Roth [21]. First, Roth's magnetic potential expression and derivation of leakage inductance per unit length is shortly recaptured in Appendix A-A and A-C for the sake of a comprehensive derivation.

A. Roth's Magnetic Potential Expression

Roth's vector potential expression assumes individual rectangular windings parallel to the core edges that carry homogeneous current density in through-plane-direction (z). The windings are embedded in the inside-window (IW) cross section with the coordinate system placed in the lower left corner of the window as shown in Fig. 9a . The boundary condition (BC) at each boundary is $\frac{\partial A_z}{\partial n} = 0$, where n represents the orthogonal direction to the boundaries. This implies infinite core permeability $\mu_{\mathrm{r,c}} \to \infty$ as these BCs lead to an orthogonal magnetic field ($\vec{n} \times \vec{H} = \vec{0}$) at the boundary.[2] With these assumptions, the current density of winding k can be represented by a 2-dimensional Fourier series according to (17).

$$J_{z,k}(x,y) = \sum_{m=0}^{\infty}\sum_{n=0}^{\infty} J_{k,mn}\cos\left(m\tfrac{\pi}{w_\mathrm{w}}x\right)\cos\left(n\tfrac{\pi}{h_\mathrm{w}}y\right) \quad (17)$$

[2]Note that the assumption of $\mu_{\mathrm{r,c}} \to \infty$ is a very good approximation in leakage inductance calculations with high permeability materials. This is because the reluctance share of air is always significantly higher than the reluctance share of the core due to the big difference in permeabilities in case of the leakage field (balanced magnetomotive forces).

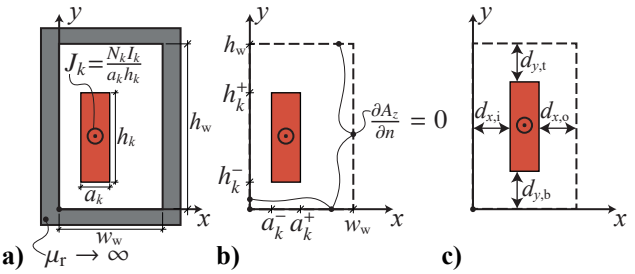

Fig. 9: **a)** Arbitrary winding k in IW cross section. **b)** Roth's mathematical problem in terms of geometry. **c)** Winding placed in the center of the core window. When modelling the OW cross section, $d_{y,\mathrm{b}}$, $d_{y,\mathrm{t}}$, $d_{x,\mathrm{o}}$ are increased to eliminate the influence of the core material.

The Fourier coefficients of the current density $J_{k,mn}$ are calculated with (18).

$$\begin{aligned}
J_{k,00} &= \tfrac{J_k}{w_\mathrm{w} h_\mathrm{w}}\left(h_k^+ - h_k^-\right)\left(a_k^+ - a_k^-\right)\\
J_{k,m0} &= \tfrac{2J_k}{m h_\mathrm{w}\pi}\left(\sin\left(\tfrac{m\pi a_k^+}{w_\mathrm{w}}\right) - \sin\left(\tfrac{m\pi a_k^-}{w_\mathrm{w}}\right)\right)\left(h_k^+ - h_k^-\right)\\
J_{k,0n} &= \tfrac{2J_k}{n w_\mathrm{w}\pi}\left(\sin\left(\tfrac{n\pi h_k^+}{h_\mathrm{w}}\right) - \sin\left(\tfrac{n\pi h_k^-}{h_\mathrm{w}}\right)\right)\left(a_k^+ - a_k^-\right)\\
J_{k,mn} &= \tfrac{4J_k}{mn\pi^2}\left(\sin\left(\tfrac{m\pi a_k^+}{w_\mathrm{w}}\right) - \sin\left(\tfrac{m\pi a_k^-}{w_\mathrm{w}}\right)\right)\\
&\qquad \left(\sin\left(\tfrac{n\pi h_k^+}{h_\mathrm{w}}\right) - \sin\left(\tfrac{n\pi h_k^-}{h_\mathrm{w}}\right)\right)
\end{aligned} \quad (18)$$

where $J_k = \frac{N_k I_k}{a_k h_k}$ is the MMF-density of winding k. All geometrical parameters are defined in Fig. 9.
The magnetic potential and the current density are connected via Poisson's equation $\nabla^2 A_z = -\mu_0 J_z$. Hence, the magnetic potential can also be represented by a 2D even Fourier series according to (19).

$$A_{z,k}(x,y) = \sum_{m=0}^{\infty}\sum_{n=0}^{\infty} A_{k,mn}\cos\left(m\tfrac{\pi}{w_\mathrm{w}}x\right)\cos\left(n\tfrac{\pi}{h_\mathrm{w}}y\right) \quad (19)$$

The Fourier coefficients of the potential $A_{k,mn}$ are calculated according to (20).

$$A_{k,mn} = \frac{\mu_0\, J_{k,mn}}{\left(\frac{m\pi}{w_\mathrm{w}}\right)^2 + \left(\frac{n\pi}{h_\mathrm{w}}\right)^2} \quad (20)$$

The model of Roth can contain an arbitrary number of windings with arbitrary currents in the window. As current density and magnetic potential only occur in linear form in the Poisson equation, the total Fourier coefficients of the problem are found by superposition as shown in (21)

$$J_{mn} = \sum_{k=1}^{K} J_{k,mn} \qquad A_{mn} = \sum_{k=1}^{K} A_{k,mn} \quad (21)$$

where K is the number of all windings in the core window.

B. Simplifications for Centered Winding Positions

When windings are placed in the center of the core window regarding a specific axis, the Fourier coefficients $J_{k,mn}$ representing the periodicity in the particular direction with odd index become zero. Referring to Fig. 9c, i.e.

$$\begin{aligned}
J_{k,mn} &= 0 \qquad \text{if } d_{y,\mathrm{b}} = d_{y,\mathrm{t}} \;\&\; n \text{ is odd}\\
J_{k,mn} &= 0 \qquad \text{if } d_{x,\mathrm{i}} = d_{x,\mathrm{o}} \;\&\; m \text{ is odd}
\end{aligned}$$

For the chosen exemplary geometry with concentric windings shown in Fig. 1a, this is usually true for the y-direction. The windings are designed such that they cover as much of the core window height as possible to maximise the filling factor. A minimum distance for dielectric insulation is required, meaning the top and bottom distance from winding to yoke is small and equal. With the coordinate system chosen in Fig. 9c, this yields

$$\begin{aligned}
d_{y,\mathrm{b}} &= d_{y,\mathrm{t}}\\
h_k^- &= d_{y,b}\\
h_k^+ &= h_\mathrm{w} - d_{y,t} = h_\mathrm{w} - d_{y,b}
\end{aligned}$$

Consequently, the difference of sine functions in the first section can be reformulated in the following way.

$$J_{k,mn} \propto \sin\left(\frac{n\pi h_k^+}{h_\mathrm{w}}\right) - \sin\left(\frac{n\pi h_k^-}{h_\mathrm{w}}\right) = -\left((-1)^n + 1\right)\sin\left(\frac{n\pi d_{y,b}}{h_\mathrm{w}}\right) \underbrace{=}_{n \text{ is odd}} 0$$

C. Derivation of Magnetic Energy Per Unit Length from Roth's Potential Expression

Roth derived the magnetic energy per unit length of the 2D cross section using (9). This leads to an integration of a multiplication of two double-sums according to (22)

$$W'_\mathrm{mag} = \frac{1}{2}\iint_\mathrm{window} \left[\sum_{m=0}^{\infty}\sum_{n=0}^{\infty} A_{mn}\cos\left(m\tfrac{\pi}{w_\mathrm{w}}x\right)\cos\left(n\tfrac{\pi}{h_\mathrm{w}}y\right)\right] \left[\sum_{p=0}^{\infty}\sum_{q=0}^{\infty} J_{pq}\cos\left(p\tfrac{\pi}{w_\mathrm{w}}x\right)\cos\left(q\tfrac{\pi}{h_\mathrm{w}}y\right)\right] \mathrm{d}A \tag{22}$$

From here, our derivation is targeted on numerical implementation of the model. We can rewrite the product of the two double sums as quadruple sums as $A_{k,mn}$ is independent of p and q and $J_{k,pq}$ is independent of m and n. Furthermore, We can reverse the integration and sum and we receive (23).

$$W'_\mathrm{mag} = \frac{1}{2}\sum_{m=0}^{\infty}\sum_{n=0}^{\infty}\sum_{p=0}^{\infty}\sum_{q=0}^{\infty} A_{mn}J_{pq} \int_0^{w_\mathrm{w}}\cos\left(m\tfrac{\pi}{w_\mathrm{w}}x\right)\cos\left(p\tfrac{\pi}{w_\mathrm{w}}x\right)\mathrm{d}x \int_0^{h_\mathrm{w}}\cos\left(n\tfrac{\pi}{h_\mathrm{w}}y\right)\cos\left(q\tfrac{\pi}{h_\mathrm{w}}y\right)\mathrm{d}y \tag{23}$$

The integrals in (23) are easy to solve and many of them are 0 due to orthogonality as shown in (24).

$$\int_0^{w_\mathrm{w}}\cos\left(m\tfrac{\pi}{w_\mathrm{w}}x\right)\cos\left(p\tfrac{\pi}{w_\mathrm{w}}x\right)\mathrm{d}x = \begin{cases} w_\mathrm{w}/2 & \text{if } m = p > 0 \\ w_\mathrm{w} & \text{if } m = p = 0 \\ 0 & \text{if } m \neq p \end{cases} \tag{24}$$

Of course, the y-integrals can be solved accordingly. With this information, we can express the magnetic energy per unit length according to Roth as (25).

$$W'_\mathrm{mag} = \frac{w_\mathrm{w}h_\mathrm{w}}{2}\left[A_{00}J_{00} + \frac{1}{2}\sum_{m=1}^{\infty}A_{m0}J_{m0} + \frac{1}{2}\sum_{n=1}^{\infty}A_{0n}J_{0n} + \frac{1}{4}\sum_{m=1}^{\infty}\sum_{n=1}^{\infty}A_{mn}J_{mn}\right] \tag{25}$$

In leakage inductance calculations, the terms J_{00} and A_{00} become zero due to the balanced magnetomotive forces of the windings. The expression of the magnetic energy per unit length contains infinite series. However, the series converge rapidly with $1/m^4$. Hence, the amount of sum terms can be cancelled at a finite index, which is shown in section IV-C. A more detailed summary of Roth's potential expression and L'_σ-calculation can be found in the supplementary document of [4] and a compact but complete outline on Roth's work can be found in [27].

D. Derivation of Magnetic Energy Per Unit Angle from Roth's potential

This section contains the proposed derivation of the magnetic energy per unit angle W''_mag from Roth's potential. As introduced in section III-B, W''_mag is derived from the integral of the radially weighted magnetic energy density (10) that leads to the two integrals to be solved in (11). Note that $A_{00} = J_{00} = 0$ due to the balanced magnetomotive forces will be spared in the total derivation.
Inserting Roth's potential expression into (11) leads to the fundamental problem in (26) that will be solved here.

$$W''_\mathrm{mag} = \frac{1}{2}\left[\int_0^{h_\mathrm{w}}\int_{\frac{d_\mathrm{leg}}{2}}^{\frac{d_\mathrm{leg}}{2}+w_\mathrm{w}} x \left(\sum_{m=0}^{\infty}\sum_{n=0}^{\infty} A_{mn}\cos\left(m\tfrac{\pi}{w_\mathrm{w}}(x - d_\mathrm{leg}/2)\right)\cos\left(n\tfrac{\pi}{h_\mathrm{w}}y\right)\right) \left(\sum_{p=0}^{\infty}\sum_{q=0}^{\infty} J_{pq}\cos\left(p\tfrac{\pi}{w_\mathrm{w}}(x - d_\mathrm{leg}/2)\right)\cos\left(q\tfrac{\pi}{h_\mathrm{w}}y\right)\right)\mathrm{d}x\mathrm{d}y - \frac{1}{2\mu}\left(\int_0^{h_\mathrm{w}}\int_{\frac{d_\mathrm{leg}}{2}}^{\frac{d_\mathrm{leg}}{2}+w_\mathrm{w}} \frac{\partial}{\partial x} \left[\left(\sum_{m=0}^{\infty}\sum_{n=0}^{\infty} A_{mn}\cos\left(m\tfrac{\pi}{w_\mathrm{w}}(x - d_\mathrm{leg}/2)\right)\cos\left(n\tfrac{\pi}{h_\mathrm{w}}y\right)\right) \left(\sum_{p=0}^{\infty}\sum_{q=0}^{\infty} A_{pq}\cos\left(p\tfrac{\pi}{w_\mathrm{w}}(x - d_\mathrm{leg}/2)\right)\cos\left(q\tfrac{\pi}{h_\mathrm{w}}y\right)\right)\mathrm{d}x\mathrm{d}y\right)\right]\right] \tag{26}$$

Note that the coordinate origin needs to be placed at the rotational axis as shown in Fig. 1b to acquire the corrected magnetic energy per unit angle and (26) is formulated in accordance with this coordinate system.
As next step, we transform the coordinate system such that the origin coincides with the coordinate system used in Roth's potential expression (cf. Fig. 9), which results in (27).

$$W''_\mathrm{mag} = \frac{1}{2}\left[\int_0^{h_\mathrm{w}}\int_0^{w_\mathrm{w}}\left(x + \frac{d_\mathrm{leg}}{2}\right) \left(\sum_{m=0}^{\infty}\sum_{n=0}^{\infty} A_{mn}\cos\left(m\tfrac{\pi}{w_\mathrm{w}}x\right)\cos\left(n\tfrac{\pi}{h_\mathrm{w}}y\right)\right) \left(\sum_{p=0}^{\infty}\sum_{q=0}^{\infty} J_{pq}\cos\left(p\tfrac{\pi}{w_\mathrm{w}}x\right)\cos\left(q\tfrac{\pi}{h_\mathrm{w}}y\right)\right)\mathrm{d}x\mathrm{d}y - \frac{1}{2\mu}\left(\int_0^{h_\mathrm{w}}\int_0^{w_\mathrm{w}} \frac{\partial}{\partial x} \left[\left(\sum_{m=0}^{\infty}\sum_{n=0}^{\infty} A_{mn}\cos\left(m\tfrac{\pi}{w_\mathrm{w}}x\right)\cos\left(n\tfrac{\pi}{h_\mathrm{w}}y\right)\right) \left(\sum_{p=0}^{\infty}\sum_{q=0}^{\infty} A_{pq}\cos\left(p\tfrac{\pi}{w_\mathrm{w}}x\right)\cos\left(q\tfrac{\pi}{h_\mathrm{w}}y\right)\right)\mathrm{d}x\mathrm{d}y\right)\right]\right] \tag{27}$$

The above equation (27) contains two double integrals. The first one is referred to as "radially weighted integral", the second one will be called "squared potential integral".

1) Solution of Radially Weighted Integral: As in the derivation of the magnetic energy per unit length, integrals and sums can be switched and the x- and y-integrals can be separated, resulting in (28)

$$\sum_{m=0}^{\infty}\sum_{n=0}^{\infty}\sum_{p=0}^{\infty}\sum_{q=0}^{\infty} A_{mn}J_{pq}\int_0^{h_\mathrm{w}}\cos\Big(n\tfrac{\pi}{h_\mathrm{w}}y\Big)\cos\Big(q\tfrac{\pi}{h_\mathrm{w}}y\Big)\,\mathrm{d}y \int_0^{w_\mathrm{w}}\Big(x+\frac{d_\mathrm{leg}}{2}\Big)\cos\Big(m\tfrac{\pi}{w_\mathrm{w}}x\Big)\cos\Big(p\tfrac{\pi}{w_\mathrm{w}}x\Big)\,\mathrm{d}x. \tag{28}$$

To solve the y-integral in (28), relation (24) is used. Fundamental solutions of the x-integral are given in (29).

$$\int_0^{w_\mathrm{w}} x\ \cos\Big(m\tfrac{\pi}{w_\mathrm{w}}x\Big)\cos\Big(p\tfrac{\pi}{w_\mathrm{w}}x\Big)\ \mathrm{d}x = \begin{cases} \frac{w_\mathrm{w}^2}{2} & \text{if } m=p=0 \\ \frac{w_\mathrm{w}^2}{4} & \text{if } m=p\geq 1 \\ -\frac{2w_\mathrm{w}^2}{\pi^2}\frac{1}{p^2} & \text{if } m\neq p\wedge m=0\wedge p \text{ is odd} \\ -\frac{2w_\mathrm{w}^2}{\pi^2}\frac{1}{m^2} & \text{if } m\neq p\wedge p=0\wedge m \text{ is odd} \\ -\frac{2w_\mathrm{w}^2}{\pi^2}\frac{m^2+p^2}{(m^2-p^2)^2} & \text{if } m\neq p\wedge m\geq 1\wedge p\geq 1\wedge m+p \text{ is odd} \\ 0 & \text{else} \end{cases} \tag{29}$$

Inserting the solutions of the integrals and reformulating yields the solution of the radially weighted integral shown in (30).

$$(28) = d_\mathrm{leg}W'_\mathrm{mag} + \frac{h_\mathrm{w}w_\mathrm{w}^2}{4}\left[\sum_{m=1}^{\infty}A_{m0}K_{m0}+\sum_{n=1}^{\infty}A_{0n}K_{0n}+\frac{1}{2}\sum_{m=1}^{\infty}\sum_{n=1}^{\infty}A_{mn}K_{mn}\right] \tag{30}$$

with

$$K_{m0} = J_{m0} - \frac{8}{\pi^2}\sum_{\substack{p=1\\ m+p \text{ is odd}}}^{\infty} J_{p0}\frac{m^2+p^2}{(m^2-p^2)^2}$$

$$K_{0n} = J_{0n} - \frac{8}{\pi^2}\sum_{p \text{ is odd}}^{\infty}\frac{J_{pn}}{2p^2}\left(1+\frac{n^2w_\mathrm{w}^2}{n^2w_\mathrm{w}^2+p^2h_\mathrm{w}^2}\right)$$

$$K_{mn} = J_{mn} - \frac{8}{\pi^2}\sum_{\substack{p=1\\ m+p \text{ is odd}}}^{\infty} J_{pn}\frac{m^2+p^2}{(m^2-p^2)^2}$$

2) Solution of Squared Potential Integral: The second double integral in (27) can be rewritten as (31)

$$\sum_{m=0}^{\infty}\sum_{n=0}^{\infty}\sum_{p=0}^{\infty}\sum_{q=0}^{\infty} A_{mn}A_{pq}\int_0^{w_\mathrm{w}}\frac{\partial}{\partial x}\cos\Big(m\tfrac{\pi}{w_\mathrm{w}}x\Big)\cos\Big(p\tfrac{\pi}{w_\mathrm{w}}x\Big)\,\mathrm{d}x \int_0^{h_\mathrm{w}}\cos\Big(n\tfrac{\pi}{h_\mathrm{w}}y\Big)\cos\Big(q\tfrac{\pi}{h_\mathrm{w}}y\Big)\,\mathrm{d}y. \tag{31}$$

Where

$$\int_0^{w_\mathrm{w}}\frac{\partial}{\partial x}\cos\Big(m\tfrac{\pi}{w_\mathrm{w}}x\Big)\cos\Big(p\tfrac{\pi}{w_\mathrm{w}}x\Big)\,\mathrm{d}x = (\cos(m\pi)\cos(p\pi)-1) = \begin{cases}-2 & \text{if } m+p \text{ is odd}\\ 0 & \text{if } m+p \text{ is even}\end{cases}. \tag{32}$$

With (32) and (24), the solution of (31) can be written as (33)

$$(31) = -2h_\mathrm{w}\left[\sum_{\substack{m=1\\ m+p \text{ is odd}}}^{\infty}\sum_{p=1}^{\infty}A_{m0}A_{p0}+\sum_{\substack{n=1\\ p \text{ is odd}}}^{\infty}\sum_{p=1}^{\infty}A_{0n}A_{pn} +\frac{1}{2}\sum_{m=1}^{\infty}\sum_{\substack{n=1\\ m+p \text{ is odd}}}^{\infty}\sum_{p=1}^{\infty}A_{mn}A_{pn}\right]. \tag{33}$$

3) Total Magnetic Energy Per Unit Angle: With the solutions of the two double integrals at hand, the total magnetic energy per unit angle can be formulated as (34).

$$W''_\mathrm{mag} = \frac{h_\mathrm{w}w_\mathrm{w}^2}{8}\left[\sum_{m=1}^{\infty}A_{m0}\tilde{J}_{m0}+\sum_{n=1}^{\infty}A_{0n}\tilde{J}_{0n}+\frac{1}{2}\sum_{m=1}^{\infty}\sum_{n=1}^{\infty}A_{mn}\tilde{J}_{mn}\right] \tag{34}$$

with

$$\tilde{J}_{m0} = \left(\frac{d_\mathrm{leg}}{w_\mathrm{w}}+1\right)J_{m0} + \frac{8}{\pi^2}\sum_{\substack{p=1\\ m+p \text{ is odd}}}^{\infty}\left(\frac{1}{2p^2}-\frac{m^2+p^2}{(m^2-p^2)^2}\right)J_{p0}$$

$$\tilde{J}_{0n} = \left(\frac{d_\mathrm{leg}}{w_\mathrm{w}}+1\right)J_{0n} + \frac{8}{\pi^2}\sum_{\substack{p=1\\ p \text{ is odd}}}^{\infty}\left(\frac{h_\mathrm{w}^2}{p^2h_\mathrm{w}^2+n^2w_\mathrm{w}^2}-\frac{1}{p^2}\left(1+\frac{n^2w_\mathrm{w}^2}{p^2h_\mathrm{w}^2+n^2w_\mathrm{w}^2}\right)\right)\frac{J_{pn}}{2}$$

$$\tilde{J}_{mn} = \left(\frac{d_\mathrm{leg}}{w_\mathrm{w}}+1\right)J_{mn} + \frac{8}{\pi^2}\sum_{\substack{p=1\\ m+p \text{ is odd}}}^{\infty}\left(\frac{1}{2}\frac{h_\mathrm{w}^2}{p^2h_\mathrm{w}^2+n^2w_\mathrm{w}^2}-\frac{m^2+p^2}{(m^2-p^2)^2}\right)J_{pn} \tag{35}$$

Finally, the leakage inductance p.u.a. is calculated with the proposed magnetic energy p.u.a. from (34) using (4).

APPENDIX B
HYBRID DOUBLE-2D LEAKAGE INDUCTANCE MODEL

The Hybrid Double-2D (HD2D) uses the Double-2D modelling concept introduced in section II-A and consists of carefully selected existing submodels shown in Tab. VIII for the required quantities. The HD2D model is simpler than the HQ3D model in some regards. However, the HD2D model has two restrictions:

- The geometry is restricted to 2 concentric windings.

Table VIII: Submodels of the Hybrid Double-2D (HD2D) model.

Quantity	Chosen submodel	Reference
$L'_{\sigma,\mathrm{IW}}$	Roth (13)	[21]
$L'_{\sigma,\mathrm{OW}}$	Margueron et al. 2010	[22]
$l_{\sigma,\mathrm{IW}}$	Empirically Corrected Axial Flux (ECAF)*	[5]
$l_{\sigma,\mathrm{OW}}$	Empirically Corrected Axial Flux (ECAF)*	[5]

*Axial Flux model [5], if $\frac{(h_1+h_2)/2}{d+(a_1+a_2)/3} > 20$ or $\frac{d}{(a_1+a_2)/3} > 5$

Table IX: Validity range of ECAF model [5]. See Figs. 1b&c for parameter definitions.

$\frac{h_1-h_2}{\frac{1}{2}(h_1+h_2)}$	$\frac{h_1-h_2}{2(d+(a_1+a_2)/3)}$	$\frac{d}{(a_1+a_2)/3}$	$\frac{\max(a_1,a_2)}{\min(a_1,a_2)}$	$\frac{(h_1+h_2)/2}{d+(a_1+a_2)/3}$
0–0.5	0–4	0.6–5	1–5	1.06–20

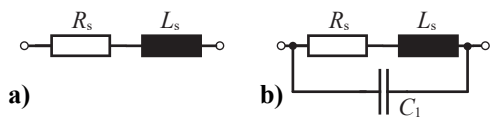

Fig. 10: **a)** R_sL_s-equiv. circuit. **b)** $R_sL_sC_p$-equiv. circuit.

- The validity range is restricted to geometries within the boundaries given in Tab. IX due to the empirical nature of the ECAF model [5] that is used for calculating the leakage length (3).

The selection and limitations of the submodels are shortly explained in the following: The IW and OW leakage inductances per unit length are calculated with Roth's model [21] and Margueron's model [22] just as in the HQ3D model as they are best suitable regarding accuracy and computational effort [4].

For IW and OW leakage lengths, the Empirically Corrected Axial Flux (ECAF) model [5] is selected due to its high accuracy and simple implementation. The ECAF model follows an empirical approach to take into account the curvature of the magnetic field at curved winding sections. Further details on its derivation can be found in [5]. The advantage of the ECAF model is that it only consists of a single equation. The disadvantage is that the ECAF correction is empirical. Therefore, the correction ceases to be valid in geometries, in which the radial flux components heavily exceed the axial flux components and in geometries, in which mainly axial flux is present. For the latter ($^{(h_1+h_2)/2}/_{d+(a_1+a_2)/3} > 20$ and $^{d}/_{(a_1+a_2)/3} > 5$), the ordinary axial flux model (without empirical correction) should be used (cf. Tab. VIII).

Appendix C
Compensation of First Resonant Capacitance

To obtain frequency dependent inductances, the magnitude of the impedance Z and the impedance phase angle φ of the device under test (DUT) are measured over frequency. Then, an R_sL_s-equivalent circuit as shown in Fig. 10a is assumed and the resulting apparent inductance is acquired via its transfer function according to (36)

$$L_{\text{apparent}} = {}^{1}/_{(2\pi f)} Z \sin(\varphi) \tag{36}$$

However, as soon as the first resonance is approached (cf. Fig. 11a), the R_sL_s-equivalent circuit is no longer an accurate representation of the DUT. Here, the impedance is mainly capacitive and the apparent inductance from (36) is therefore erroneous as is clearly visible in Fig. 11b, in which the apparent inductance even becomes negative after the resonance.

To extract the actual inductance in the region of the first resonance shown in Fig. 8, the influence of the first resonant capacitance C_1 is eliminated by estimating the capacitance

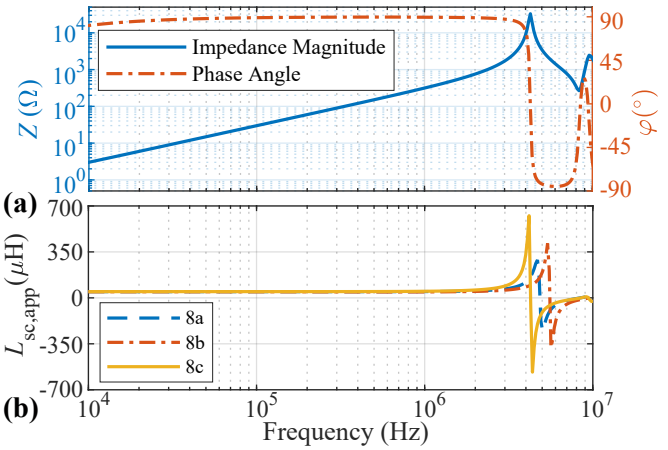

Fig. 11: **a)** First resonance of transformer No.8c at around 5 MHz. **b)** Apparent short-circuit inductance (36) increase close to the first resonance due capacitively dominated regime.

via the undamped resonance frequency $C_1 = {}^{1}/_{(2\pi f_{\text{res}})^2 L_{\text{static}}}$ where L_{static} is the static low frequency inductance. Finally, the inductance is calculated from the $R_sL_sC_p$-equivalent circuit (Fig. 10b) according to (37).

$$L = -\frac{R_s - Z\,e^{j\varphi}\,(1 + j\,C_1\,R_s\,\omega)}{\omega\,(C_1\,Z\,\omega\,e^{j\varphi} + j)} \tag{37}$$

References

[1] D. Leuenberger and J. Biela, "PV-Module-Integrated AC Inverters (AC Modules) with Subpanel MPP Tracking," *IEEE Trans. on Power Electronics*, vol. 32, no. 8, pp. 6105–6118, 2017.

[2] D. Dujic, F. Kieferndorf, F. Canales, and U. Drofenik, "Power electronic traction transformer technology," in *Conf. Proc. of IEEE International Power Electronics and Motion Control Conference - ECCE Asia, IPEMC*, 2012, pp. 636–642.

[3] J. Biela and J. W. Kolar, "Pareto-optimal design and performance mapping of telecom rectifier concepts," in *Proc. of the Power Conversion and Intelligent Motion (PCIM) Conf.*, Shanghai, 2010.

[4] R. Schlesinger and J. Biela, "Comparison of Analytical Models of Transformer Leakage Inductance: Accuracy vs. Computational Effort," *IEEE Trans. on Power Electronics*, vol. 36, no. 1, pp. 146–156, 2021.

[5] ——, "Leakage Inductance Modelling of Transformers: Accurate and Fast Models to Scale the Leakage Inductance Per Unit Length," in *Proc. of European Conf. on Power Electronics and Applications (EPE ECCE Europe)*, Lyon, 2020.

[6] G. Kapp, *Transformatoren für Wechselstrom und Drehstrom*, 3rd ed. Birmingham: Springer, 1907.

[7] P. Dowell, "Effects of eddy currents in transformer windings," *Proc. of the Institution of Electrical Engineers*, vol. 113, no. 8, p. 1387, 1966.

[8] P. Wallmeier, "Generalization of Orthogonality Principle to model solenoidal wound multiwinding transformers," in *IEEE Ind. App. Conf. 36th IAS Annual Meeting*. Chicago: IEEE, 2001.

[9] M. A. Bahmani and T. Thiringer, "Accurate Evaluation of Leakage Inductance in High Frequency Transformers Using an Improved Frequency-Dependent Expression," *IEEE Transactions on Power Electronics*, vol. 30, no. 10, pp. 5738–5745, 2015.

[10] Z. Ouyang, J. Zhang, and W. G. Hurley, "Calculation of Leakage Inductance for High-Frequency Transformers," *IEEE Transactions on Power Electronics*, vol. 30, no. 10, pp. 5769–5775, 2015.

[11] A. K. Das, Z. Wei, S. Cao, S. Vaisambhayana, H. Tian, A. Tripathi, and P. C. Kjær, "Accurate calculation of leakage inductance for balanced and fractional-interleaved winding in medium-frequency high-power transformer," in *IEEE Southern Power Electronics Conference, SPEC*, Puerto Varas, 2017.

[12] Z. Ouyang, W. G. Hurley, and M. A. E. Andersen, "Improved Analysis and Modelling of Leakage Inductance for Planar Transformers," *IEEE Journal of Emerging and Selected Topics in Power Electronics*, vol. 7, no. 4, pp. 2225–2231, 2019.

[13] R. Prieto, J. A. Cobos, O. García, P. Alou, and J. Uceda, "Study of 3-D magnetic components by means of "Double 2-D" methodology," *IEEE Trans. on Industrial Electronics*, vol. 50, no. 1, pp. 183–192, 2003.
[14] M. Mogorovic and D. Dujic, "100 kW, 10 kHz Medium-Frequency Transformer Design Optimization and Experimental Verification," *IEEE Trans. on Power Electronics*, vol. 34, no. 2, pp. 1696–1708, 2019.
[15] A. Fouineau, M. A. Raulet, B. Lefebvre, N. Burais, and F. Sixdenier, "Semi-Analytical Methods for Calculation of Leakage Inductance and Frequency-Dependent Resistance of Windings in Transformers," *IEEE Trans. on Magnetics*, vol. 54, no. 10, 2018.
[16] X. Guo, C. Li, Z. Zheng, and Y. Lia, "A General Analytical Model and Optimization for Leakage Inductances of Medium-Frequency Transformers," *IEEE Journal of Emerging and Selected Topics in Power Electronics*, vol. Early Acce, 2021.
[17] M. Eslamian, M. Kharezy, and T. Thiringer, "An Accurate Analytical Method for Leakage Inductance Calculation of Shell-Type Transformers With Rect. Windings," *IEEE Access*, vol. 9, pp. 72 647–72 660, 2021.
[18] L. Rabins, "Transformer reactance calculations with digital computers," *Transactions of the American Institute of Electrical Engineers, Part I: Communication and Electronics*, vol. 75, no. 3, pp. 261–267, 1956.
[19] M. Eslamian, M. Kharezy, and T. Thiringer, "An Accurate Method for Leakage Inductance Calculation of Shell-Type Multi Core-Segment Transformers with Circular Windings," *IEEE Access*, vol. 9, pp. 111 417 – 111 431, 2021.
[20] A. Sharma and J. W. Kimball, "Evaluation of Transformer Leakage Inductance Using Magnetic Image Method," *IEEE Transactions on Magnetics*, vol. 57, no. 11, 2021.
[21] E. Roth, "Étude analytique du champ de fuites des transformateurs et des efforts mécaniques exercés sur les enroulements," *Revue générale de l'électricité*, vol. 23, pp. 773–787, 1928.
[22] X. Margueron, A. Besri, P. O. Jeannin, J. P. Keradec, and G. Parent, "Complete analytical calculation of static leakage parameters: A step toward HF transformer optimization," *IEEE Trans. on Industry Applications*, vol. 46, no. 3, pp. 1055–1063, 2010.
[23] L. Råde and B. Westergren, *Mathematics Handbook for Science and Engineering*, 3rd ed. Springer, 1995.
[24] J. D. Jackson, *Classical Electrodynamics*, 3rd ed. Wiley, 1999.
[25] W. Rogowski, "Ueber das Streufeld und den Streuinduktionskoeffizienten eines Transformators mit Scheibenwicklung und geteilten Endspulen," Ph.D. dissertation, Technische Hochschule zu Danzig, 1908.
[26] X. Margueron, J. P. Keradec, and D. Magot, "Analytical calculation of static leakage inductances of HF transformers using PEEC formulas," *IEEE Trans. on Industry Applications*, vol. 43, no. 4, pp. 884–892, 2007.
[27] P. Hammond, "Roth's method for the solution of boundary-value problems in electrical engineering," *Proceedings of the Institution of Electrical Engineers*, vol. 114, no. 12, pp. 1969–1976, 1967.

Richard Schlesinger (S'19) Richard Schlesinger is pursuing his PhD degree at the Laboratory for High Power Electronic Systems at ETH Zurich since 2018. His research interests include modelling and design of magnetic components with special focus on analytical modelling of the transformer leakage inductance. Richard received the Dipl.-Ing. degree (MSc equivalent) with distinction from TU Wien, Austria in energy and environmental technology in 2018. In his master's thesis he modelled and evaluated three-terminal impedance measurement setups for solid oxide fuel cell electrodes. During his studies, he spent exchange semesters at the UPC in Barcelona and at Beuth UAS in Berlin and worked with the Austrian Institute of Technology.

Thomas Ewald (Student Member, IEEE) studied electrical engineering with focus on Energy Conversion Technology at Technical University of Munich (TUM) in Germany. He received his B.Sc. and M.Sc. degree from TUM in 2015 and 2018, respectively. In 2017, he wrote his Master's Thesis at BMW AG in the R&D department for electrical drive components. In his Master's thesis he developed an analytical model for simulating transient processes in both, permanent magnet and electrically excited synchronous machines. Since November 2019 he is a Ph.D. student at the Laboratory for High Power Electronic Systems (HPE) at ETH Zurich, working on analytical inductor models and automated optimization processes.

Jürgen Biela (S'04-M'06-SM'16) received the Diploma (Hons.) degree from Friedrich-Alexander Universität Erlangen-Nürnberg, Germany, in 1999, and the Ph.D. degree from the Swiss Federal Institute of Technology (ETH) Zürich, Switzerland, in 2006. In 2000, he joined the research department, Siemens A&D, Erlangen, Germany, and in 2002, he joined the Power Electronic Systems Laboratory, ETH Zürich, as Ph.D. student focusing on electromagnetically integrated resonant converters. From 2006 to 2010, he was a Postdoctoral Fellow with the Power Electronic Systems Laboratory. Since 2010, he is an Associate Professor and since 2020, Full Professor of High-Power Electronic Systems (HPE) with ETH Zurich.